IEEE Access
Multidisciplinary | Rapid Review | Open Access Journal

Received October 10, 2019, accepted October 20, 2019, date of publication October 23, 2019, date of current version November 7, 2019.

*Digital Object Identifier 10.1109/ACCESS.2019.2949197*

# Integral Fuzzy Sliding Mode Impedance Control of an Upper Extremity Rehabilitation Robot Using Time Delay Estimation

**QINGCONG WU, (Member, IEEE), DAWEN XU, BAI CHEN, AND HONGTAO WU**
College of Mechanical and Electrical Engineering, Nanjing University of Aeronautics and Astronautics, Nanjing 210016, China

Corresponding author: Qingcong Wu (wuqc@nuaa.edu.cn)

This work was supported in part by the National Natural Science Foundation of China under Grant 51705240, in part by the Natural Science Foundation of Jiangsu Province of China under Grant BK20170783, in part by the State Key Laboratory of Robotics and System (HIT) under Grant SKLRS-2018-KF-10, and in part by the China Postdoctoral Science Foundation under Grant 2019T120425.

**ABSTRACT** Robot-assisted cooperative rehabilitation training has shown superiority in helping the individuals with motion impairment problems to regain their motor functions. This paper presents the development and evaluation of a new cooperative training control scheme for an end-effector-type rehabilitation robot to provide upper extremity rehabilitation training with desired compliance and intensity. Firstly, the overall mechanical structure and real-time control system of rehabilitation robot are introduced. Secondly, an integral fuzzy sliding mode impedance control strategy combined with time-delay estimation (IFSMIC-TDE) is proposed to induce the active participation of patients and suppress impedance error. The IFSMIC-TDE approach is free from nonlinear robot dynamics, and it is designed to be robust to the external uncertainties and inherent chattering characteristics. After that, the closed-loop system stability with IFSMIC-TDE is proved based on the Lyapunov stability theory. Finally, experimental investigations are conducted to illustrate the effectiveness of the proposed rehabilitation robot and control algorithm. The comparison results indicate that the proposed IFSMIC-TDE can achieve better control performance and less impedance error. Besides, the interaction compliance and training intensity can be qualitatively adjusted via appropriate impedance parameters.

**INDEX TERMS** Upper extremity rehabilitation robot, cooperative training, sliding mode impedance control, fuzzy turner, time delay estimation.

## I. INTRODUCTION

With the rapid increase of the elderly and stroke population, more and more individuals are suffering from motor disorder problem. These people urgently require effective and long-term rehabilitation training to improve muscle strength and regain motor function. In traditional clinical therapy, physical therapists need to manually assist the disabled patients to perform repetitive training based on their personal experience and skill. However, there exist many inherent shortcomings in the conventional manual treatment, such as high labor intensity, high treatment expense, poor sustainability and limited professional therapist resources [1].

The associate editor coordinating the review of this manuscript and approving it for publication was Mohsin Jamil.

In recent decades, robot-assisted rehabilitation training have received much attention from around the world due to its promising potential in medical application. Therapeutic robots can provide programmable high-efficiency and long-endurance rehabilitation training in accordance with the specific recovery progress and condition of patients. Besides, the treatment effectiveness can be precisely monitored and recorded in real-time via integrated sensing system, which facilitates the optimization of therapy schemes [2]. Generally, rehabilitation robots can be categorized into two types based on their interaction capacities. One is the end-effector-type rehabilitation robot [3]–[9], which has only a human-robot interaction point at the robot end-effector. Another is the exoskeleton-type rehabilitation robot [10]–[15], which can be worn on the human extremity with multiple connected points.

Clinical research results have demonstrated the effectiveness of robot-assisted therapies over traditional rehabilitation approaches [16], [17].

In practical implementation, the control strategies applied in rehabilitation robots directly determine the performance of robot-assisted rehabilitation training [18]. Currently, the existing rehabilitation control schemes can be classified into two types according to the participation degree of patients, i.e., the passive training control strategies [19]–[21] for the patients at the acute period to passively conduct repetitive movement tasks along predefined trajectory, and the cooperative training control strategies [22]–[26] for the patients at the recovery period to be actively engaged in the therapy training program. In [27], a passive training control approach combined with neuron proportion-integral and feedforward compensation control was developed to reduce the trajectory tracking error of a pneumatic muscles-driven rehabilitation robot. In [28], an enhanced neural-network-based repetitive learning controller was proposed for a lower limb exoskeleton to improve control accuracy and human safety during trajectory tracking training. In [29], a dynamics-based fuzzy sliding mode controller was designed to guarantee the control accuracy and frequency response property of an upper extremity exoskeleton in passive rehabilitation training. In [30], an adaptive integral terminal sliding mode controller was developed to deal with the dynamic uncertainties of an upper limb rehabilitation exoskeleton. In [31], an adaptive fuzzy controller was proposed to ensure the control accuracy of an end-effector-type cable-driven rehabilitation robot.

Compared with the passive training mode, the cooperative training focuses on enhancing the compliance of human-robot interaction and encouraging the active participation of patients. In [32], a minimal assist-as-needed controller was developed based on sensorless force estimation, which can promotes the recovery of motor coordination in robotic rehabilitation protocol. In [33], a novel adaptive high-level admittance control scheme was implemented on a compliant ankle rehabilitation robot to ensure the cooperative training safety. In [34], a coordination impedance control approach combined with human stiffness transfer disturbance observer was developed for robotic exoskeleton. In [35], a minimal-intervention-based admittance control strategy was proposed for exoskeleton-assisted rehabilitation training based on coupled interaction dynamics. In [36], a voltage-based robust impedance control scheme combined with an adaptive fuzzy estimator was developed for lower-limb rehabilitation robot. In [37], [38], the impedance characteristics of human arm are estimated and used to adjust the controller parameters of an end-effector-type rehabilitation robot. In [39], an adaptive neural network force/position hybrid controller was designed for an end-effector robot called PAM to provide compliant rehabilitation training.

Conventional model-based controllers of rehabilitation robots require accurate calculation of nonlinear dynamics. Nevertheless, the computational complexity, external disturbance as well as the parametric uncertainties of muscles severely degrade the control performance of these model-based schemes. The time-delay estimation (TDE) technique provides a simple yet highly effective strategy to estimate and compensate the nonlinear and uncertain terms of robot dynamics from previous state response and control output [40]. The TDE-based controllers with compact structures are robust against external disturbances, modeling error, and parameters variation. TDE has been successfully applied in many robotic systems to realize mode-free control, such as autonomous underwater vehicle [41], robot manipulator [42], unmanned aerial vehicles [43], robotic exoskeleton [44], [45], multilateral teleoperation system [46], and series elastic actuators [47]. However, the TDE errors resulted from the measurement noise of discrete signals along sampling time would deteriorate the performance of time delay controllers during operation [44].

Taking the above into consideration, compared with the existing works, the significance and innovation of this paper focus on the development of a new integral sliding mode impedance control strategy integrated with fuzzy adjustment and time delay estimation for an upper limb rehabilitation robot to assist the disabled individuals perform cooperative training. Based on the TDE approach, the proposed IFSMIC-TDE scheme is capable of estimating and compensating the external uncertainties and modeling errors without accurate knowledge of dynamic model parameters. The integral fuzzy sliding mode controller is proposed to restrain the TDE error and chattering phenomenon and, moreover, achieve desired impedance dynamics. The interaction compliance can be adjust to encourage active patient participation. The system stability are formulated and demonstrated via the Lyapunov functional theory. Three different experiments are carried out to evaluate the effectiveness of the proposed rehabilitation robot and IFSMIC-TDE control algorithm.

The reminder of this paper is organized as follows. Section II presents the developed upper extremity rehabilitation robot. In Section III, the IFSMIC-TDE control strategy as well as its stability analysis are presented and discussed. In Section IV, the conducted experiments are described and the experimental results are presented. Section V concludes this study and gives a forecast of our future works.

## II. UPPER EXTREMITY REHABILITATION ROBOT

### A. MECHANICAL DESIGN

The architecture and major mechanical components of the developed upper extremity rehabilitation robot are presented in Fig. 1. The end-effector-type therapeutic robotic device is designed as a planar mechanism to realize the multi-joins rehabilitation training of human shoulder, wrist, and elbow simultaneously. The robotic system consists a bottom support platform to adjust the location and height of entire equipment, and an upper mobile platform to generate translational and rotational movements on horizontal plane. More specifically, it has two active translational degrees of freedom (DOF), which are mutually perpendicular to each other, along the

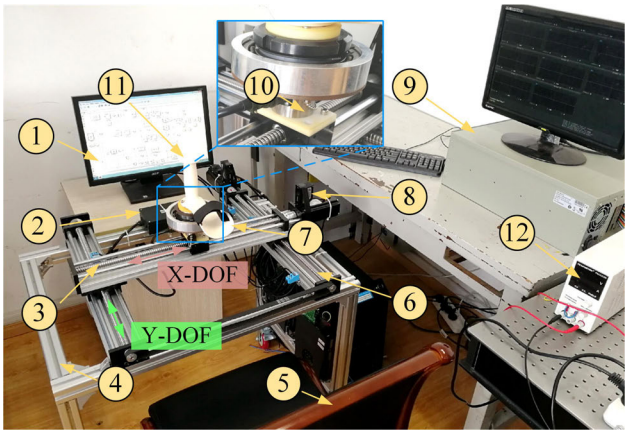


**FIGURE 1.** Architecture and major components of the upper extremity rehabilitation robot (1-Guidance monitor; 2-Amplifier; 3-Mobile platform; 4-Support platform; 5-Chair; 6-Ball screw mechanisms; 7-End-effector; 8-Laser sensor; 9-RTW control system; 10-Force sensor; 11-Operating handle; 12-Power supply).

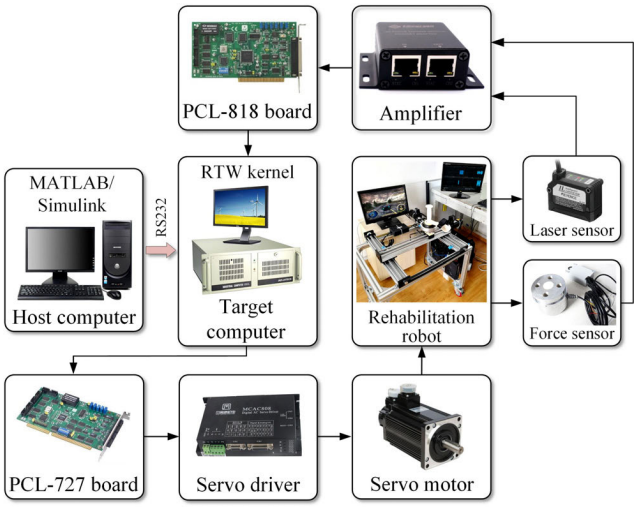


**FIGURE 2.** Diagram of the established MATLAB/Simulink/xPC real-time control system.

anteroposterior direction (Y-DOF) and bilateral direction (X-DOF) to adjust the end-position of biological arm. In addition, there is a passive revolute DOF located at the robot end-effector to modulate the configuration of forearm relative to mobile platform. The rehabilitation robot is highly adjustable to satisfy the upper limb training requirement of patients with different anthropometry parameters and affected sides (both right arm and left arm). Two high-precision linear ball screw mechanisms (G1610, FUYU) driven by alternating current servo motors (RH-400, RENHOU) are installed in the therapeutic device to provide active movement assistance in the horizontal direction. The range of motion (ROM) of the developed rehabilitation robot is designed to basically cover the horizontal ROM of human in activities of daily living. A customized operating handle with a soft Velcro strap is mounted on the end-effector to facilitate the patients to interact with the robotic rehabilitation system. A torsional spring is encapsulated into the end-effector for the purpose of promoting the interaction compliance of passive rotary DOF. During rehabilitation training, the patient first needs to sit on the chair in front of the robot with his/her hand grasping the operating handle, and then carry out predefined training tasks with the therapeutic device.

A three-axis force sensors (LZ-SWL2, KINO, resolution: 0.05 N) is mounted at the bottom of end-effector to obtain the human-robot interaction forces in Cartesian space. Two laser sensors (IL-600, KEYENCE, accuracy: 50 $\mu$m) are installed on the fixed frame of ball screw mechanisms to measure the horizontal position of end-effector. An angular potentiometer (MNA-992, MINUO) is integrated into end-effector to detect the rotation angle of revolute joint. The system status and the game-like training interface are displayed on a guidance monitor to provoke active participation of patients. Four position-limit switches are used to restrict the ROM of ball screw mechanisms and protect the patients from excessive movements. Two dead-man buttons are integrated into the robot system, which allow patient and physical therapist to rapidly turn off the power supply in the case of emergency.

### B. ELECTRICAL REAL-TIME CONTROL SYSTEM

The control system of the rehabilitation robot is established based on the MATLAB/Simulink/RTW (2016a, Mathworks) real-time kernel and the xPC target operating environment. The real-time property of control system directly influences the practical control performance of robot. The RTW system provides a combination of code generation facilities with an available real-time execution environment for the practical control of robot. The overall diagram of the real-time control system is shown in Fig. 2. The system has two industrial personal computers (IPC-610H, Advantech) working as the upper-layer host computer generating executable codes and the lower-layer target computer implementing the target-specific codes, respectively [48]. The RS232 serial port is utilized to realize the connection between host and target computers. An industrial analog-to-digital board (PCL-818, Advantech) is installed into the target computer to acquire the feedback signals from force/torque sensor, linear laser sensors and potentiometer. In addition, a digital-to-analog board (PCL-727, Advantech) is also installed into the target computer, which is in charge of converting the digital control commands into corresponding analog signals. The output analog control commands are sent to the servo drivers to modulate the running of motors. The sampling period of the host control layer and target control layer are all set to 1 ms.

## III. DEVELOPMENT OF IFSMIC-TDE STRATEGY

Clinical rehabilitation training experience indicates that the passive training mode is particularly suitable for the patients without any motor functions to motivate muscle contraction and avoid further deterioration. However, for the disabled individuals who have regained parts of motor functions but still be weak, the cooperative training mode combined with

the active interaction and motion intention of patient shows better therapeutic outcomes when compared with the passive training mode. Thus, a new integral sliding mode impedance controller combined with fuzzy adjustment and time-delay estimation is developed to assist patient conduct cooperative treatment with adjustable training compliance and intensity.

### A. CONTROLLER DESIGN

The desired impedance dynamics of human-robot interaction can be described as:

$$\mathbf{M}_{\mathrm{d}}\Delta\ddot{\mathbf{P}}(t)+\mathbf{B}_{\mathrm{d}}\Delta\dot{\mathbf{P}}(t)+\mathbf{K}_{\mathrm{d}}\Delta\mathbf{P}(t)=\Gamma(t) \tag{1}$$

where

$$\Delta\mathbf{P}(t)=\mathbf{P}_{\mathrm{d}}(t)-\mathbf{P}(t). \tag{2}$$

Here, $\mathbf{M}_{\mathrm{d}}$, $\mathbf{B}_{\mathrm{d}}$, and $\mathbf{K}_{\mathrm{d}} \in R^{2\times2}$ denote the objective inertial matrix, damping matrix, and stiffness matrix of the impedance model. $\Gamma(t) \in R^2$ represents the interaction forces in Cartesian space. $\mathbf{P}_{\mathrm{d}}(t)$ and $\mathbf{P}(t) \in R^2$ denote the desired position and actual position of end-effector. $\Delta\mathbf{P}(t)$, $\Delta\dot{\mathbf{P}}(t)$, and $\Delta\ddot{\mathbf{P}}(t) \in R^2$ are the position error, velocity error, and acceleration error of end-effector in Cartesian space.

The overall dynamic model of the rehabilitation robot combined with human-robot interaction can be established on the basis of Lagrangian dynamic equation [35]:

$$\boldsymbol{\tau}(t)=\mathbf{M}\ddot{\mathbf{P}}(t)+\mathbf{V}\dot{\mathbf{P}}(t)+\mathbf{F}_f(t)+\mathbf{D}_u(t)-\boldsymbol{\Gamma}(t) \tag{3}$$

where $\mathbf{M}$ and $\mathbf{V} \in R^{2\times2}$ denote the Cartesian space inertia matrix and Coriolis/centripetal matrix. $\mathbf{F}_f(t) \in R^2$ represents the friction vector. $\mathbf{D}_u(t) \in R^2$ is the lumped effects of external uncertainties and modeling errors.

Here, it should be pointed that the dynamic model has no gravitational vector, as the available ROM of rehabilitation robot is limited to the horizontal plane.

By introducing a positive constant diagonal gain matrix $\bar{\mathbf{M}}=diag(\bar{m}_{11},\ \bar{m}_{22}) \in R^2$, (3) can be rewritten as follow:

$$\boldsymbol{\tau}(t)=\bar{\mathbf{M}}\ddot{\mathbf{P}}(t)+(\mathbf{M}-\bar{\mathbf{M}})\ddot{\mathbf{P}}(t)+\mathbf{V}\dot{\mathbf{P}}(t)+\mathbf{F}_f(t)+\mathbf{D}_u(t)-\boldsymbol{\Gamma}(t) \tag{4}$$

For the simplification of (4), defining a vector $\mathbf{N}(t) \in R^2$ to include the nonlinear terms as follow:

$$\mathbf{N}(t)=(\mathbf{M}-\bar{\mathbf{M}})\ddot{\mathbf{P}}(t)+\mathbf{V}\dot{\mathbf{P}}(t)+\mathbf{F}_f(t)+\mathbf{D}_u(t)-\boldsymbol{\Gamma}(t). \tag{5}$$

By combining (4) and (5), we can get

$$\boldsymbol{\tau}(t)=\bar{\mathbf{M}}\ddot{\mathbf{P}}(t)+\mathbf{N}(t). \tag{6}$$

Then, the time delay estimation (TDE) technique can be adopted to estimate the nonlinear $\mathbf{N}(t)$ if the delay time $L$ is sufficiently small. We can have

$$\mathbf{N}(t)\approx\hat{\mathbf{N}}(t)=\mathbf{N}(t-L)=\boldsymbol{\tau}(t-L)-\bar{\mathbf{M}}\ddot{\mathbf{P}}(t-L). \tag{7}$$

Here, $\mathbf{N}(t-L)$, $\boldsymbol{\tau}(t-L)$, and $\ddot{\mathbf{P}}(t-L)$ denote the time delayed values of $\mathbf{N}(t)$, $\boldsymbol{\tau}(t)$, and $\ddot{\mathbf{P}}(t)$ respectively. Generally, the delay time $L$ is chosen as the sampling period in practical digital implementation.

Combining (1), (6), and (7), the preliminary control input, which consists of a TDE control term and a target impedance dynamics (TID) control term, can be designed as the follow equations:

$$\boldsymbol{\tau}(t)=\hat{\mathbf{N}}(t)+\bar{\mathbf{M}}u(t)=\underbrace{\boldsymbol{\tau}(t-L)-\bar{\mathbf{M}}\ddot{\mathbf{P}}(t-L)}_{TDE\ control\ term}+\underbrace{\bar{\mathbf{M}}u(t)}_{TID\ control\ term} \tag{8}$$

$$\mathbf{u}(t)=\ddot{\mathbf{P}}_d(t)+\mathbf{M}_{\mathrm{d}}^{-1}\left[\mathbf{B}_{\mathrm{d}}\Delta\dot{\mathbf{P}}(t)+\mathbf{K}_{\mathrm{d}}\Delta\mathbf{P}(t)-\Gamma(t)\right]. \tag{9}$$

Inserting (8) and (9) into (6), we can obtain

$$\begin{aligned}&\bar{\mathbf{M}}^{-1}\left[\mathbf{N}(t)-\hat{\mathbf{N}}(t)\right]\\&=\mathbf{u}(t)-\ddot{\mathbf{P}}(t)\\&=\Delta\ddot{\mathbf{P}}(t)+\mathbf{M}_{\mathrm{d}}^{-1}\left[\mathbf{B}_{\mathrm{d}}\Delta\dot{\mathbf{P}}(t)+\mathbf{K}_{\mathrm{d}}\Delta\mathbf{P}(t)-\Gamma(t)\right].\end{aligned} \tag{10}$$

Here, the TDE error vector $\kappa(t) \in R^2$ is defined as follow

$$\kappa(t)=\bar{\mathbf{M}}^{-1}\left[\mathbf{N}(t)-\hat{\mathbf{N}}(t)\right]. \tag{11}$$

Applying (11) into (10), we have

$$\mathbf{M}_{\mathrm{d}}\boldsymbol{\kappa}(t)=\mathbf{M}_{\mathrm{d}}\Delta\ddot{\mathbf{P}}(t)+\mathbf{B}_{\mathrm{d}}\Delta\dot{\mathbf{P}}(t)+\mathbf{K}_{\mathrm{d}}\Delta\mathbf{P}(t)-\boldsymbol{\Gamma}(t). \tag{12}$$

By comparing (12) with (1), it can be observed that the TDE error will lead to the deviation between the actual impedance dynamics and desired impedance dynamics during rehabilitation training.

Therefore, a hitting control term is developed and combined into the preliminary control law shown in (8) and (9) to suppress the TDE error and achieve desired impedance dynamics.

Defining the integral sliding surface $\mathbf{s}(t)=[s_1(t),s_2(t)]^T$ as follow:

$$\mathbf{s}(t)=\int_0^t\left\{\Delta\ddot{\mathbf{P}}(\varsigma)+\mathbf{M}_{\mathrm{d}}^{-1}\left[\mathbf{B}_{\mathrm{d}}\Delta\dot{\mathbf{P}}(\varsigma)+\mathbf{K}_{\mathrm{d}}\Delta\mathbf{P}(\varsigma)-\boldsymbol{\Gamma}(\varsigma)\right]\right\}d\varsigma. \tag{13}$$

From (1), it can be found that the trajectory of sliding variable $\mathbf{s}(t)$ represents the time-varying value of impedance error [49]. According to the Barbalat's Lemma, if the sliding variable and its derivative with respect to time gradually converges to zero in finite time, the desired impedance dynamics of the closed-loop human-robot interaction system can be guaranteed.

Combining aforementioned formulations, the control law can be improved by integrating with a hitting control term as follow:

$$\begin{aligned}\boldsymbol{\tau}(t)&=\bar{\mathbf{M}}u(t)+\hat{\mathbf{N}}(t)+\mathbf{W}sat(\mathbf{s})\\&=\boldsymbol{\tau}(t-L)-\bar{\mathbf{M}}\ddot{\mathbf{P}}(t-L)+\bar{\mathbf{M}}u(t)+\mathbf{W}sat(\mathbf{s})\\&=\underbrace{\boldsymbol{\tau}(t-L)-\bar{\mathbf{M}}\ddot{\mathbf{P}}(t-L)}_{TDE\ control\ term}+\\&\quad\underbrace{\bar{\mathbf{M}}\left\{\ddot{\mathbf{P}}_d(t)+\mathbf{M}_{\mathrm{d}}^{-1}\left[\mathbf{B}_{\mathrm{d}}\Delta\dot{\mathbf{P}}(t)+\mathbf{K}_{\mathrm{d}}\Delta\mathbf{P}(t)-\Gamma(t)\right]\right\}}_{TID\ control\ term}\\&\quad+\underbrace{\mathbf{W}sat(\mathbf{s})}_{Hitting\ control\ term}\end{aligned} \tag{14}$$

Here, $\mathbf{W} = diag(w_{11}, \ w_{22}) \in R^2$ denotes a positive diagonal gain matrix.$sat(\mathbf{s})$ represents a saturation function with a dead-zone compensation expressed as follow

$$sat(s_i) = \begin{cases} \text{sign}(s_i) & \text{if } |s_i| > \varphi \\ \dfrac{(1-\rho)s_i + \rho\varphi}{\varphi} & \text{if } |s_i| \le \varphi \end{cases} \quad i = 1, 2 \tag{15}$$

where $\varphi$ denotes a positive constant defining the boundary layer thickness of the saturation function; $\rho$ represents the constant dead-zone compensation value; sign $(\cdot)$ denotes the sign function.

Inserting (11) and the improved control law (14) into (6), we can obtain

$$\mathbf{u}(t) - \ddot{\mathbf{P}}(t) + \bar{\mathbf{M}}^{-1}\mathbf{W}sat(\mathbf{s}) = \dot{\mathbf{s}}(t) + \bar{\mathbf{M}}^{-1}\mathbf{W}sat(\mathbf{s}) = \boldsymbol{\kappa}(t). \tag{16}$$

### B. STABILITY ANALYSIS

The Lyapunov stability criteria is utilized to demonstrate the closed-loop stability of the rehabilitation robot under the proposed IFSMIC-TDE control strategy. A positive-definite Lyapunov-like function candidate is selected as:

$$V(t) = \frac{1}{2}\mathbf{s}^T(t)\mathbf{s}(t) \tag{17}$$

Differentiating (17) with respect to time and combining (16), we can obtain

$$\begin{aligned} \dot{V}(t) &= \mathbf{s}^T(t)\dot{\mathbf{s}}(t) \\ &= \mathbf{s}^T(t)\left[\boldsymbol{\kappa}(t) - \bar{\mathbf{M}}^{-1}\mathbf{W}sat(\mathbf{s})\right] \\ &= -\bar{\mathbf{M}}^{-1}\mathbf{W}sat(\mathbf{s})\mathbf{s}^T(t) + \mathbf{s}^T(t)\boldsymbol{\kappa}(t) \\ &= -diag\left(\frac{w_{11}}{\bar{m}_{11}}, \frac{w_{22}}{\bar{m}_{22}}\right) sat(\mathbf{s})\mathbf{s}^T(t) + \mathbf{s}^T(t)\boldsymbol{\kappa}(t) \\ &\le -\sum_{i=1}^{2} \rho\frac{w_{ii}}{\bar{m}_{ii}}|s_i(t)| + \sum_{i=1}^{2} s_i(t)\kappa_i(t) \\ &\le -\sum_{i=1}^{2} \rho\frac{w_{ii}}{\bar{m}_{ii}}|s_i(t)| + \sum_{i=1}^{2} |s_i(t)|\,\kappa_i(t) \\ &\le -\sum_{i=1}^{2} \rho\frac{w_{ii}}{\bar{m}_{ii}}|s_i(t)| + \sum_{i=1}^{2} |s_i(t)|\,\|\kappa(t)\|_2 \\ &= -\sum_{i=1}^{2} |s_i(t)|\left[\rho\frac{w_{ii}}{\bar{m}_{ii}} - \|\boldsymbol{\kappa}(t)\|_2\right] \end{aligned} \tag{18}$$

where $\|\cdot\|_2$ represents the 2-norm of matrix.

*Lemma 1:* The TDE error $\|\kappa(t)\|_2$ is bounded by a constant $\xi$ if the following condition is satisfied [50]–[52]:

$$\left\|\mathbf{I} - \mathbf{M}^{-1}\bar{\mathbf{M}}\right\|_2 < 1 \tag{19}$$

Thus, we have

$$\|\boldsymbol{\kappa}(t)\|_2 \le \xi \tag{20}$$

If the positive parameters $w_{11}$ and $w_{22}$ of gain matrix $\mathbf{W}$ are selected as follows:

$$w_{11} \ge \frac{\xi\bar{m}_{11}}{\rho} \tag{21}$$

$$w_{22} \ge \frac{\xi\bar{m}_{22}}{\rho} \tag{22}$$

Then, by applying (21) and (22) into (18), we can have

$$\begin{aligned} \dot{V}(t) &\le -\sum_{i=1}^{2} |s_i(t)|\left[\rho\frac{w_{ii}}{\bar{m}_{ii}} - \|\boldsymbol{\kappa}(t)\|_2\right] \\ &\le -\sum_{i=1}^{2} |s_i(t)|\left[\rho\frac{w_{ii}}{\bar{m}_{ii}} - \xi\right] \\ &\le 0 \end{aligned} \tag{23}$$

It can be found that the Lyapunov function $V(t)$ is positive definite, while its derivative $\dot{V}(t)$ is negative definite. Moreover, when $\|\mathbf{s}(t)\|_2$ tends to infinity, $V(t)$ also approaches to infinity. Therefore, the proposed IFSMIC-TDE control scheme is globally asymptotically stable, and the impedance error gradually converges to zero in finite time.

### C. FUZZY ADJUSTMENT

Existing literatures [53]–[55] reveal that the sliding mode controller could lead to undesirable chattering problem when the system asymptotically reaches sliding surface, as the sign function and the saturation function of hitting control term are unsmooth. Thus, a fuzzy logic inference mechanism is integrated into the proposed controller to rationally adjust the positive diagonal gain matrix $\mathbf{W}$ of hitting control term.

The elements of matrix $\mathbf{W}$ can be redefined as a fuzzy function of sliding variable and its derivative:

$$\begin{aligned} w_{ii} &= \frac{\xi\bar{m}_{ii}}{\rho} + FUZ\left\{s_i(t), \dot{s}_i(t)\right\} \\ &= \vartheta_i + \Delta w_{ii} \quad i = 1, \ 2 \end{aligned} \tag{24}$$

where $\vartheta_i = \xi\bar{m}_{ii}/\rho$ represents the original value of $w_{ii}$; $\Delta w_{ii} = FUZ\left\{s_i(t), \dot{s}_i(t)\right\}$ is the fuzzy output adjustment value.

The fuzzy rules are determined based on the following two basic principles to decrease the chattering phenomenon:

(a) Condition:$s_i(t) \cdot \dot{s}_i(t) > 0$. In this situation, the sliding variable tends to move away from the sliding surface. Therefore, for larger $|s_i(t)|$ or larger $|\dot{s}_i(t)|$, the increase of adjustment value $\Delta w_{ii}$ helps to enforce the sliding variable to return to the sliding surface with less time.

(b) Condition:$s_i(t) \cdot \dot{s}_i(t) < 0$. In this situation, the sliding variable tends to move toward the sliding surface. Therefore, for smaller $|s_i(t)|$ or larger $|\dot{s}_i(t)|$, the decrease of adjustment value $\Delta w_{ii}$ helps to reduce the velocity passing through the sliding surface and restrain the chattering phenomenon.

The detailed description of the adopted fuzzy controller has been shown in our previous research [19]. The overall block diagram of the proposed integral fuzzy sliding mode impedance controller integrated with time delay estimation

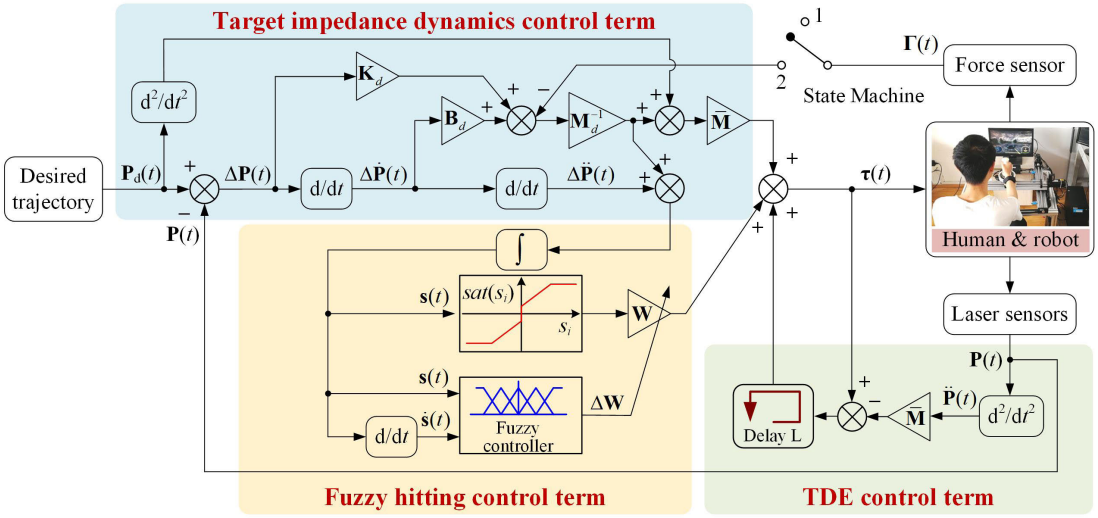


**FIGURE 3.** Overall block diagram of the proposed IFSMIC-TDE strategy.

**TABLE 1.** Characteristics of the subjects participating in the experiments.

| Subject | Age | Gender | Height | Weight |
|---|---|---|---|---|
| S1 | 23 | Male | 1.72 m | 60 kg |
| S2 | 36 | Male | 1.78 m | 68 kg |
| S3 | 53 | Female | 1.61 m | 51 kg |

is depicted in Fig. 3. It should be pointed out that the IFSMIC-TDE can be converted from the cooperative training mode to the passive training mode by switching the state machine to the "1" location and, as a result, disconnecting the interaction force feedback loop. In this situation, the compliance of human-robot interaction is eliminated during passive training. Meanwhile, the position feedback loop is still retained to ensure the trajectory tracking accuracy of passive training.

## IV. EXPERIMENTS AND RESULTS

Experimental investigations were carried out by three subjects with different heights, weights, ages and genders to evaluate the performance of the developed rehabilitation robot and IFSMIC-TDE control strategy, as shown in Table 1. In our study, three different experiments were conducted by the subjects, including the trajectory tracking experiment, the impedance-based trajectory tracking experiment, and the intention-based resistive training experiment. Fig. 4 presents the scenarios of a subject sitting in front of the therapeutic device, grasping the end-effector, and conducting the rehabilitation training experiments. The ethical approval of each experiment has been obtained from the Institutional Review Board of the Nanjing University of Aeronautics and Astronautics. Besides, all of the experimenters gave written consent to participate in the experiment programs.

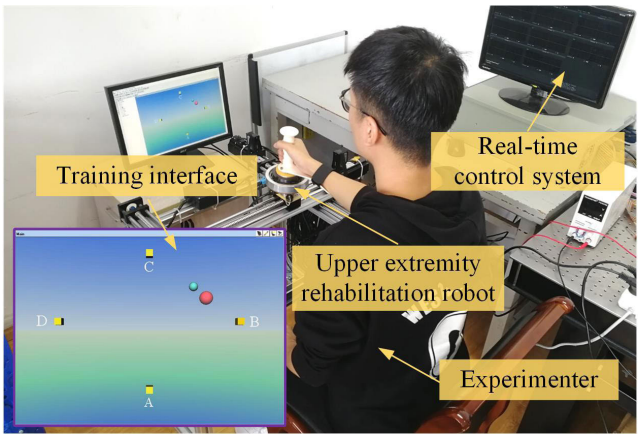


**FIGURE 4.** Photograph of upper extremity rehabilitation prototype with a subject performing experiments.

### A. TRAJECTORY TRACKING EXPERIMENT

To analyze the effectiveness of the proposed IFSMIC-TDE scheme in assisting disabled patients perform passive training, the passive trajectory tracking experiments without taking the human-robot interaction force is carried out in the first test. The state machine of the controller was switched to the passive training mode. The end-effector was controlled to track a repetitive triangular-sinusoidal-hybrid trajectory with time-varying frequency and peak-to-peak amplitude along bilateral and anteroposterior directions, simultaneously. The referenced trajectory of X-DOF has a sinusoidal trajectory with a frequency of 0.25 Hz and an amplitude of 80 mm in the first 4 s, which then change to 0.5 Hz and 60 mm in the next 4 s. From $t = 8$ s to $t = 12$ s, the reference changes to a triangular trajectory with a frequency of 0.25 Hz and an amplitude of 100 mm. In the last 4 s, the frequency and amplitude change to 0.5 Hz and 70 mm. For the Y-DOF,

the reference has a triangular trajectory with a frequency of 0.25 Hz and an amplitude of 100 mm in the first 4 s. From $t = 4$ s to $t = 8$ s, the desired trajectory changes to a sinusoidal curve with a frequency of 0.5 Hz and an amplitude of 60 mm. In the next 4 s, the frequency and amplitude change to 0.25 Hz and 80 mm. The last 4 s has a triangular trajectory with a frequency of 0.5 Hz and an amplitude of 70 mm.

To make a comparison, a model-based sliding mode impedance controller (MBSMIC) [56] was implemented in this research to evaluate the control performance of IFSMIC-TDE. The controller parameters were carefully adjusted and optimized by intensive trials to promote control performance. For a quantitative analysis, the percent root mean squared error (PRMSE) and percent maximum absolute error (PMAE) are defined as the following equations:

$$\text{PRMSE} = \frac{\sqrt{\frac{1}{n}\sum_{i=1}^{n}\Delta P_i(t)^2}}{\max\left[\mathbf{P}_d(t)\right] - \min\left[\mathbf{P}_d(t)\right]} \times 100\% \tag{25}$$

$$\text{PMAE} = \frac{\max\left(|\Delta P_i(t)|\right)}{\max\left[\mathbf{P}_d(t)\right] - \min\left[\mathbf{P}_d(t)\right]} \times 100\% \tag{26}$$

where $\Delta P_i(t)$ denotes the $i$ th position tracking error data; $n$ is the number of data sets.

In the trajectory tracking experiment, the subjects S1, S2, and S3 are all instructed to passively conduct the repetitive training respectively. The impedance parameters are set to $\mathbf{M}_d$ = diag [2.0, 2.0] N ·s$^2$/mm, $\mathbf{B}_d$ = diag [2.0, 2.0] N·s/mm, and $\mathbf{K}_d$ = diag [2.0, 2.0] N/mm, respectively. The results of the experiment performed by S1 are presented in Figs. 5 and 6. More specifically, the trajectories and tracking errors of IFSMIC-TDE and MBSMIC are compared in Figs. 5 (a)-(c) and Figs. 6 (a)-(c). It can be seen from the plots that the measured trajectories nearly overlapped with the reference, and the control accuracy of IFSMIC-TDE is higher than that of MBSMIC. For the trajectory tracking results along X-direction, the PRMSE declines from 4.65% (MBSMIC) to 2.88% (IFSMIC-TDE), while the PMAE declines from 8.62% (MBSMIC) to 4.89% (IFSMIC-TDE). For the trajectory tracking results along Y-direction, IFSMIC-TDE also achieves smaller PRMSE (2.67%) and PMAE (4.56%) when compared with those of the MBSMIC (PRMSE: 5.02%, PMAE: 8.81%). Besides, it can be observed that there exists time delay between the referenced and actual trajectories, which mainly come from the low-pass Bessel filter utilized to filter the feedback sensing signals and the practical controller property. The time delay value of IFSMIC-TDE is smaller than that of MBSMIC. Figs. 5 (d) and 6 (d) show the relation between sliding function $s_i(t)$ and its derivative $\dot{s}_i(t)$, which indicate that the convergence of IFSMIC-TDE in the phase plane is better than that of MBSMIC. The controller outputs of each control algorithms are compared in Figs. 5 (e) and 6 (e). We can observe that the chattering degree of IFSMIC-TDE is lower than that of MBSMIC. The experimental results of S1, S2, and S3 are all summarized in Table 2. It can be seen that, when compared with the MBSMIC, the IFSMIC-TDE shows better control performance during the passive mode rehabilitation training.

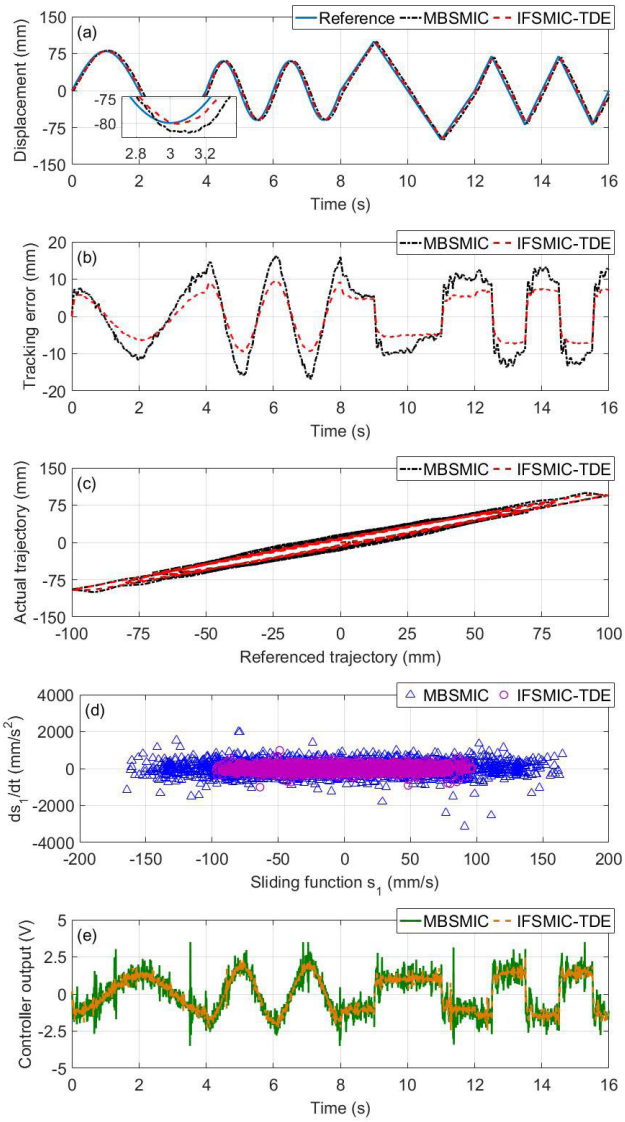


**FIGURE 5.** Results of passive trajectory tracking experiment along X-direction. (a) Time histories of reference and actual trajectories. (b) Tracking errors of MBSMIC and IFSMIC-TDE. (c) Comparison between referenced trajectory and actual trajectories. (d) Phase plane of sliding variable. (e) Controller outputs of MBSMIC and IFSMIC-TDE.

### B. IMPEDANCE-BASED TRAJECTORY TRACKING EXPERIMENT

The purpose of the impedance-based trajectory tracking experiment is to combine the feedback forces at the end-effector into trajectory tracking procedure and, furthermore, promote the human-robot interaction compliance, comfort, and safety during rehabilitation training. In this case, the state machine of the controller was switched to the cooperative training mode to enable the active interaction of patients. The desired trajectory of end-effector was defined to follow

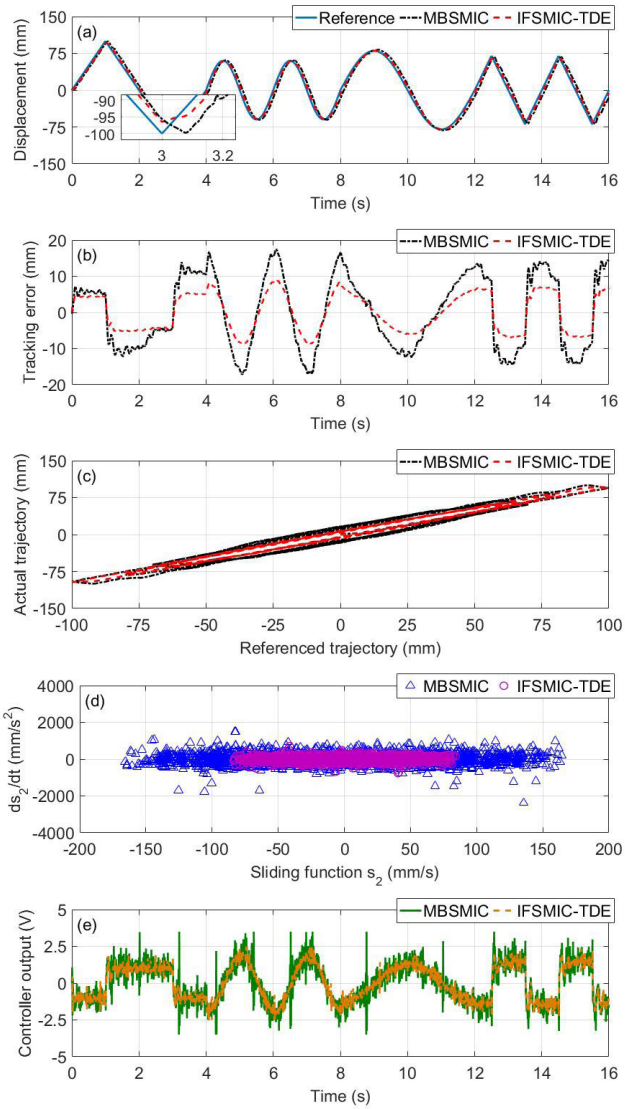


**FIGURE 6.** Results of passive trajectory tracking experiment along Y-direction. (a) Time histories of reference and actual trajectories. (b) Tracking errors of MBSMIC and IFSMIC-TDE. (c) Comparison between referenced trajectory and actual trajectories. (d) Phase plane of sliding variable. (e) Controller outputs of MBSMIC and IFSMIC-TDE.

**TABLE 2.** Statistical results of the passive trajectory tracking experiments with different control strategies and experimenters.

| Subject | Controller | X-DOF | | Y-DOF | |
|---|---|---|---|---|---|
| | | PRMSE (%) | PMAE (%) | PRMSE (%) | PMAE (%) |
| S1 | MBSMIC | 4.65 | 8.62 | 5.02 | 8.81 |
| | IFSMIC-TDE | 2.88 | 4.89 | 2.67 | 4.56 |
| S2 | MBSMIC | 4.59 | 8.70 | 5.11 | 8.93 |
| | IFSMIC-TDE | 2.93 | 4.95 | 2.80 | 4.64 |
| S3 | MBSMIC | 4.72 | 8.57 | 5.23 | 8.77 |
| | IFSMIC-TDE | 2.83 | 4.83 | 2.75 | 4.51 |

a rectangular trajectory on the horizontal plane in counter-clockwise direction for two cycles, as shown in the Fig. 7 (a). The circle time was set to 8 s. With the IFSMIC-TDE scheme, the actual training trajectory can be modulated in accordance with the real-time interaction forces applied by human hand and the predefined impedance parameters. It helps to improve interaction compliance during cooperative training. With the aim of evaluating the control performance of IFSMIC-TDE scheme, the MBSMIC strategy was also implemented in this experiment to make a comparison analysis. Three different groups of impedance parameters were adopted in the experiments to analyze the influence of impedance parameters on the cooperative rehabilitation training, as shown in Table 3.

The impedance-based trajectory tracking experiments were conducted by all of the three subjects respectively. During experiment, the experimenter was instructed to grasp the robot end-effector with his/her right hand and, moreover, intentionally apply interaction forces with certain range to adjust the training path during trajectory tracking process. The results of the experiment conducted by S1 are shown in Figs. 7-9. More specifically, Figs. 7 (a)−9 (a), Figs. 7 (b)−9 (b) and Figs. 7 (c)−9 (c) compare the referenced trajectory with the actual trajectories under MBSMIC and IFSMIC-TDE schemes. Figs. 7 (d)−9 (d) and Figs. 7 (e)−9 (e) present the relation between the resultant interaction force and the corresponding position deviation of end-effector under MBSMIC and IFSMIC-TDE schemes, respectively. In order to quantitatively analyze the human-robot interaction compliance, the comprehensive compliance level (CCL) is defined as follow:

$$\mathrm{CCL} = \frac{\sqrt{\frac{1}{n}\sum_{i=1}^{n}\Delta P_i(t)^2}}{\sqrt{\frac{1}{n}\sum_{i=1}^{n}\Gamma_i(t)^2}} \tag{27}$$

where $\Gamma_i(t)$ denotes the $i$th resultant interaction force data.

In the experiment with large impedance, the CCL of MBSMIC and IFSMIC-TDE are 0.33 mm/N and 0.27 mm/N. In the experiment with medium impedance, the CCL changes to 0.55 mm/N (MBSMIC) and 0.58 mm/N (IFSMIC-TDE). The experiment with low impedance produces the largest CCL (MBSMIC: 1.08 mm/N, IFSMIC-TDE: 1.02 mm/N). It can be concluded from the experimental results that the comprehensive interaction compliance level increases with the decrease of impedance parameters during training.

The time history of impedance errors i.e., the 2-norm of sliding variable vector, of different control strategies are compared in Figs. 7 (f)−9 (f). The mean impedance errors (MIE) of the experiment with large impedance are 102.21 mm/s (MBSMIC) and 58.64 mm/s (IFSMIC-TDE). In the experiment with medium impedance, the MIE are 174.29 mm/s (MBSMIC) and 81.25 mm/s (IFSMIC-TDE). In the experiment with low impedance, the MIE of MBSMIC and IFSMIC-TDE change to 279.51 mm/s and 122.67 mm/s. It can be observed that the IFSMIC-TDE scheme can achieve smaller impedance errors when compared with the MBSMIC scheme. Furthermore, the impedance error increases with the decreases of impedance parameters as well as the interaction

**TABLE 3. The results of impedance-based trajectory tracking experiments.**

| Experimental condition | Impedance parameters | | | Subject | MBSMIC | | IFSMIC-TDE | |
|---|---|---|---|---|---|---|---|---|
| | $\mathbf{M}_d$ (N·s$^2$/mm) | $\mathbf{B}_d$ (N·s/mm) | $\mathbf{K}_d$ (N/mm) | | CCL (mm/N) | MIE (mm/s) | CCL (mm/N) | MIE (mm/s) |
| Large impedance | diag [2.0, 2.0] | diag [2.0, 2.0] | diag [2.0, 2.0] | $S_1$ | 0.33 | 102.21 | 0.27 | 58.64 |
| | | | | $S_2$ | 0.31 | 105.70 | 0.29 | 56.15 |
| | | | | $S_3$ | 0.32 | 101.15 | 0.31 | 59.27 |
| Medium impedance | diag [0.7, 0.7] | diag [0.7, 0.7] | diag [0.7, 0.7] | $S_1$ | 0.55 | 174.29 | 0.58 | 81.25 |
| | | | | $S_2$ | 0.59 | 169.84 | 0.61 | 83.06 |
| | | | | $S_3$ | 0.56 | 172.30 | 0.55 | 85.39 |
| Low impedance | diag [0.3, 0.3] | diag [0.3, 0.3] | diag [0.3, 0.3] | $S_1$ | 1.08 | 279.51 | 1.02 | 122.67 |
| | | | | $S_2$ | 1.12 | 283.68 | 1.10 | 127.15 |
| | | | | $S_3$ | 1.06 | 273.02 | 1.04 | 128.36 |

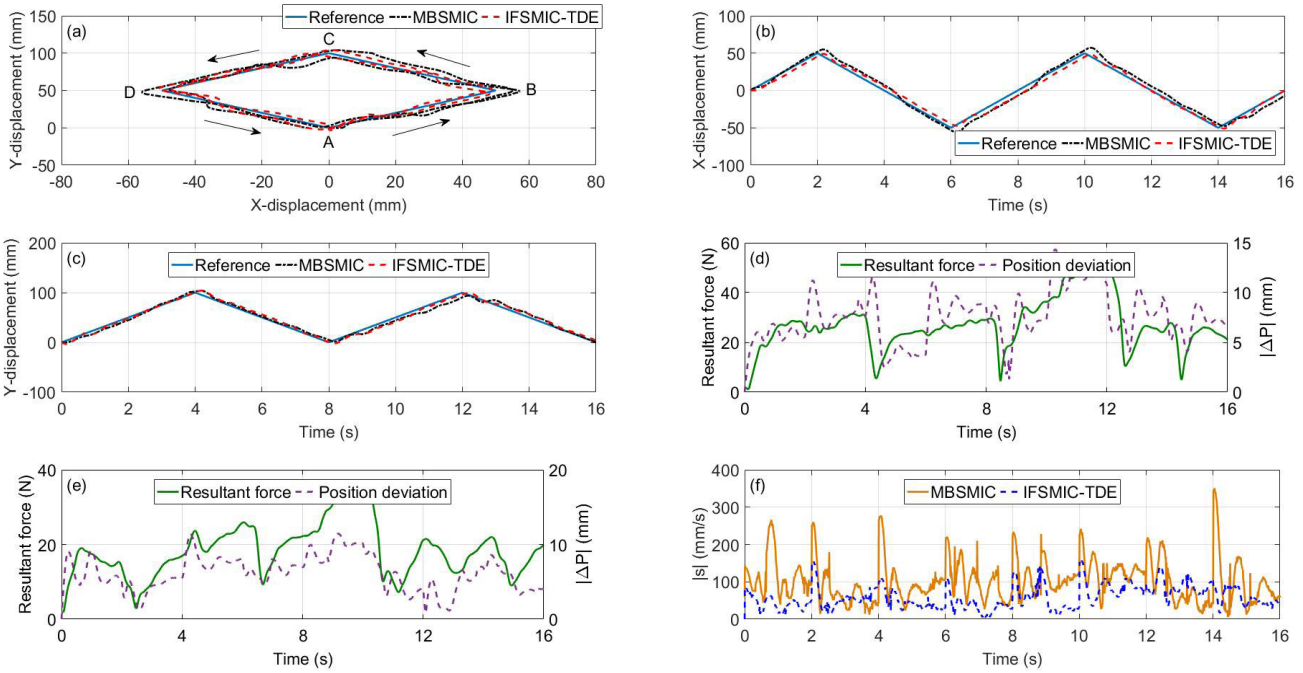


**FIGURE 7. Results of the impedance-based rectangular trajectory tracking experiments with large impedance parameters. (a) Comparison between reference and actual trajectories. (b) Time histories of reference and actual trajectories along X-direction. (c) Time histories of reference and actual trajectories along Y-direction. (d) Resultant interaction force and the corresponding position deviation of MBSMIC. (e) Resultant interaction force and the corresponding position deviation of IFSMIC-TDE. (f) Impedance errors of MBSMIC and IFSMIC-TDE.**

compliance. The statistical experimental results of subjects S1, S2, and S3 are all summarized in Table 3. The results indicate that, with the proposed IFSMIC-TDE strategy, the interaction compliance level can be rationally and accurately modulated to satisfy the rehabilitation training requirement of patients in different recovery progress.

### C. INTENTION-BASED RESISTIVE TRAINING EXPERIMENT

The purpose of the interaction-based resistive experiment is to evaluate the performance of the proposed IFSMIC-TDE scheme in enabling patients to actively conduct cooperative rehabilitation training based on human motion intention. This training mode shows positive effects in inducing the active participation of patients and, furthermore, promoting psychological confidence and recovery efficiency. The state machine of IFSMIC-TDE was switched to the cooperative training mode in this experiment. The desired trajectory was defined to remain in the original position of end-effector on the horizontal working plane. Firstly, the experimenters were instructed to sit on the front chair and grasp the operating handle with a comfortable configuration. And then, the experimenters needed to actively apply forces to the end-effector and conduct the repetitive planar movement based on their own motion intention. In this situation, the actual rehabilitation training trajectory is steered by the active movement of human hand which reflects the active human

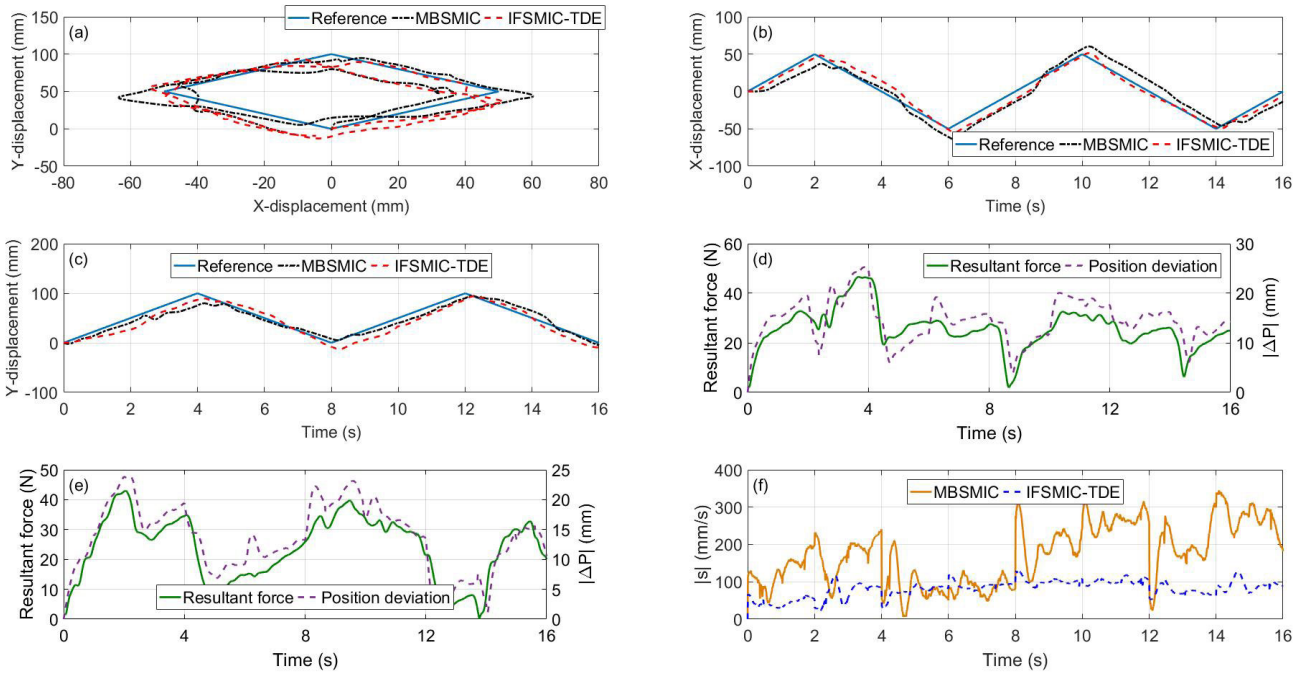


**FIGURE 8.** Results of the impedance-based rectangular trajectory tracking experiments with medium impedance parameters. (a) Comparison between reference and actual trajectories. (b) Time histories of reference and actual trajectories along X-direction. (c) Time histories of reference and actual trajectories along Y-direction. (d) Resultant interaction force and the corresponding position deviation of MBSMIC. (e) Resultant interaction force and the corresponding position deviation of IFSMIC-TDE. (f) Impedance errors of MBSMIC and IFSMIC-TDE.

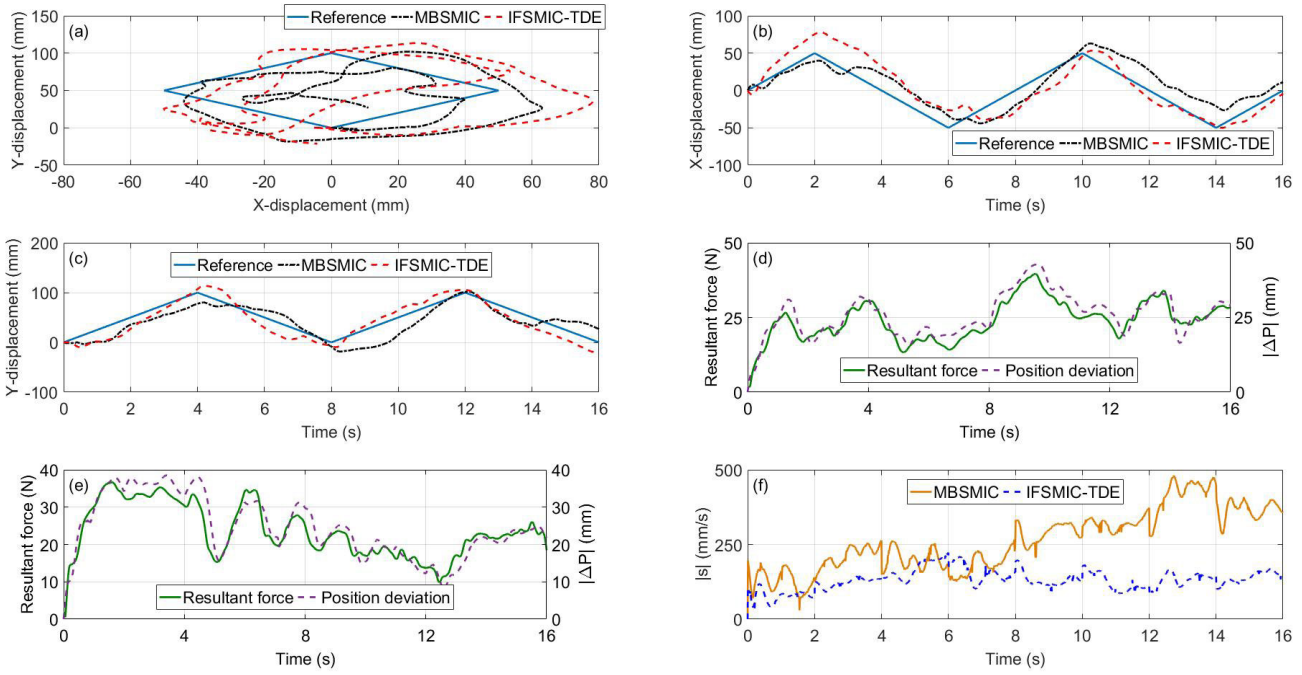


**FIGURE 9.** Results of the impedance-based rectangular trajectory tracking experiments with low impedance parameters. (a) Comparison between reference and actual trajectories. (b) Time histories of reference and actual trajectories along X-direction. (c) Time histories of reference and actual trajectories along Y-direction. (d) Resultant interaction force and the corresponding position deviation of MBSMIC. (e) Resultant interaction force and the corresponding position deviation of IFSMIC-TDE. (f) Impedance errors of MBSMIC and IFSMIC-TDE.

motion intention. The movement of end-effector is consistent with the human-robot interaction forces along corresponding direction. Meanwhile, the resistive forces exerting by the end-effector can impede the active movement of human arm according to the predefined impedance characteristics. That conduces to adjusting the training intensity of

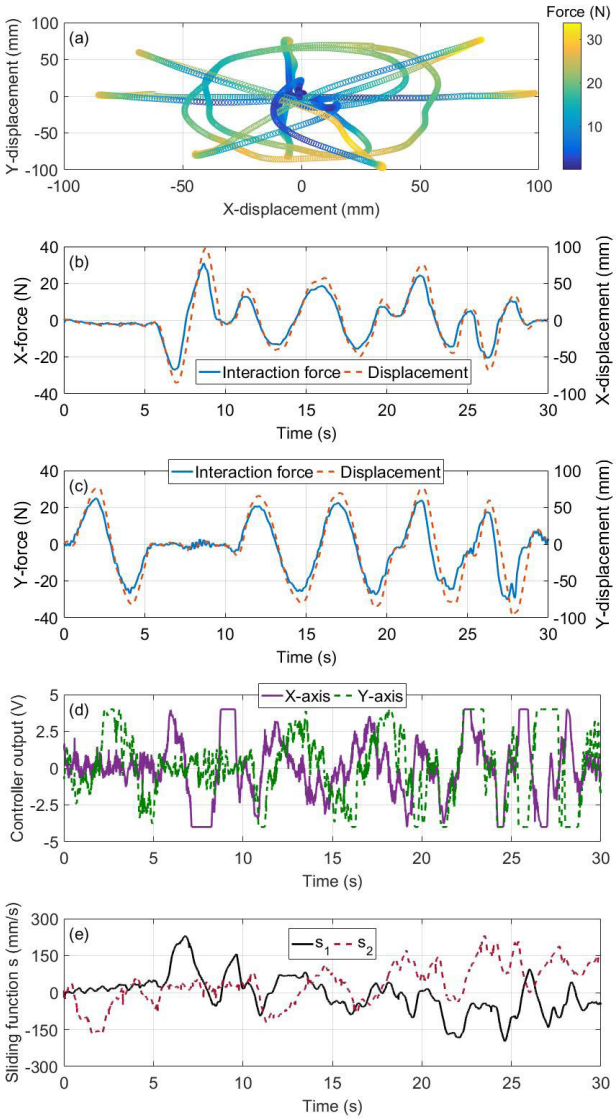


**FIGURE 10.** Results of the intention-based resistive training experiment. (a) Trajectory of end-effector and resultant interaction force. (b) Relation between the interaction force and position deviation along X-direction. (c) Relation between the interaction force and position deviation along Y-direction. (d) Controller outputs. (e) Time history of sliding variables.

patient with specific compliance level during rehabilitation training.

In this experiment, the impedance parameters were set to $\mathbf{M}_d$ = diag [0.15, 0.15] N·s$^2$/mm, $\mathbf{B}_d$ = diag [0.15, 0.15] N·s/mm, and $\mathbf{K}_d$ = diag [0.15, 0.15] N/mm, respectively. The experimenter was commanded to conduct the active training along anteroposterior direction, bilateral direction, diagonal direction, and circular path in turn. The time of duration of each experiment was set to 30 s. Fig. 10 presents the results of the experiment carried out by S1. More specifically, Fig. 10 (a) shows the trajectory of end-effector on the horizontal plane and the resultant interaction force. The time history of interaction force and the corresponding position deviation along X-DOF and Y-DOF directions are compared in Figs. 10 (b) and (c). The controller outs for each servo motor are presented in Fig. 10 (d). The time history of the sliding variables are presented in Fig. 10 (e). The experimental results demonstrate the feasibility of proposed IFSMIC-TDE strategy in providing intention-based cooperative training. The interaction force shows high consistency with the displacement in each direction. The resultant interaction force increases with the position deviation during the free-motion test. In practical application, the resistive force, which reflects the training intension, can be adjust by selecting rational impedance parameters. In addition, the advanced man-machine interface integrated with the virtual-reality or augmented-reality technologies can be applied in the intention-based resistive training mode to further improve the interestingness and immersion of training.

## V. CONCLUSION

This paper focuses on investigating the integral fuzzy sliding mode impedance control incorporating the time delay estimation for an upper extremity therapeutic robot to provide cooperative rehabilitation training. The mechanical structure and real-time control system of the rehabilitation robot are presented. The proposed IFSMIC-TDE consists of three control terms, including TDE control term, TID control term, and hitting control term. TDE term enables the analysis and compensation of nonlinear dynamic terms and external uncertainties without accurate dynamic modeling. TID and hitting control terms are capable of suppressing TDE error and achieving desired impedance dynamics. A fuzzy logic controller is utilized to reduce the chattering level of sliding mode control. The stability of closed-loop control algorithm has been verified in theory based on the Lyapunov analysis. The effectiveness of the IFSMIC-TDE were validated via trajectory tracking experiment, impedance-based trajectory tracking experiment, and intention-based resistive training experiment. The comparison results with MBSMIC strategy indicate that the IFSMIC-TDE can achieve higher control accuracy, lower chattering degree and less impedance error during training. Moreover, the interaction compliance and training intension can be adjusted by changing the impedance parameters to meet the treatment requirement of different patients. As part of our continuing work, we are working on building a virtual visualization environment to facilitate the evaluation of the robotic assistance performance and the optimization of controller parameters.

## REFERENCES

[1] R. P. Van Peppen, G. Kwakkel, S. Wood-Dauphinee, H. J. Hendriks, P. J. Van der Wees, and J. Dekker, "The impact of physical therapy on functional outcomes after stroke: What's the evidence?" *Clin Rehabil.*, vol. 18, no. 8, pp. 833–862, Dec. 2004.

[2] G. B. Prange, M. J. A. Jannink, C. G. M. Groothuis-Oudshoorn, H. J. Hermens, and M. J. Ijzerman, "Systematic review of the effect of robot-aided therapy on recovery of the hemiparetic arm after stroke," *J. Rehabil. Res. Dev.*, vol. 43, no. 2, pp. 171–184, Mar/Apr. 2006.

[3] S. Pareek, H. Manjunath, E. T. Esfahani, and T. Kesavadas, "MyoTrack: Realtime estimation of subject participation in robotic rehabilitation using sEMG and IMU," *IEEE Access*, vol. 7, pp. 76030–76041, 2019.

[4] E. P. Washabaugh, J. Guo, C.-K. Chang, C. D. Remy, and C. Krishnan, "A portable passive rehabilitation robot for upper-extremity functional resistance training," *IEEE Trans. Biomed. Eng.*, vol. 66, no. 2, pp. 496–508, Feb. 2018.

[5] V. Crocher, J. Fong, T. J. Bosch, Y. Tan, I. Mareels, and D. Oetomo, "Upper limb deweighting using underactuated end-effector-based backdrivable manipulanda," *IEEE Robot. Autom. Lett.*, vol. 3, no. 3, pp. 2116–2122, Jul. 2018.

[6] Y. Liu, C. Li, L. Ji, S. Bi, X. Zhang, J. Huo, and R. Ji, "Development and implementation of an end-effector upper limb rehabilitation robot for hemiplegic patients with line and circle tracking training," *J. Healthcare Eng.*, vol. 2017, Jun. 2017, Art. no. 4931217.

[7] M. Zhang, A. McDaid, A. J. Veale, Y. Peng, and S. Q. Xie, "Adaptive trajectory tracking control of a parallel ankle rehabilitation robot with joint-space force distribution," *IEEE Access*, vol. 7, pp. 85812–85820, 2019.

[8] F. S. di Luzio, D. Simonetti, F. Cordella, S. Miccinilli, S. Sterzi, F. Draicchio, and L. Zollo, "Bio-cooperative approach for the human-in-the-loop control of an end-effector rehabilitation robot," *Frontiers Neurorobot.*, vol. 12, p. 67, Oct. 2018.

[9] M. Hennes, K. Bollue, and H. Arenbeck, "A proposal for patient-tailored supervision of movement performance during end-effector-based robot-assisted rehabilitation of the upper extremities," *Biomed. Eng.*, vol. 60, no. 3, pp. 193–197, Jun. 2015.

[10] B. Chen, C.-H. Zhong, X. Zhao, H. Ma, L. Qin, and W.-H. Liao, "Reference joint trajectories generation of CUHK-EXO exoskeleton for system balance in walking assistance," *IEEE Access*, vol. 7, pp. 33809–33821, 2019.

[11] P. Yang, X. Ma, J. Wang, G. Zhang, Y. Zhang, and L. Chen, "Disturbance observer-based terminal sliding mode control of a 5-DOF upper-limb exoskeleton robot," *IEEE Access*, vol. 7, pp. 62833–62839, 2019.

[12] Q.-C. Wu, X. S. Wang, and F. P. Du, "Analytical inverse kinematic resolution of a redundant exoskeleton for upper-limb rehabilitation," *Int. J. Hum. Robot.*, vol. 13, no. 3, Sep. 2016, Art. no. 1550042.

[13] D. Buongiorno, E. Sotgiu, D. Leonardis, S. Marcheschi, M. Solazzi, and A. Frisoli, "WRES: A novel 3 DoF wrist exoskeleton with tendon-driven differential transmission for neuro-rehabilitation and teleoperation," *IEEE Robot. Autom. Lett.*, vol. 3, no. 3, pp. 2152–2159, Jul. 2018.

[14] D. Copaci, F. Martín, L. Moreno, and D. Blanco, "SMA based elbow exoskeleton for rehabilitation therapy and patient evaluation," *IEEE Access*, vol. 7, pp. 31473–31484, 2019.

[15] Q. C. Wu, X. S. Wang, B. Chen, and H. Wu, "Patient-active control of a powered exoskeleton targeting upper limb rehabilitation training," *Frontiers Neurol.*, vol. 8, p. 817, Oct. 2018.

[16] G. Kwakkel, B. J. Kollen, and H. I. Krebs, "Effects of robot-assisted therapy on upper limb recovery after stroke: A systematic review," *Neurorehabil. Neural Repair*, vol. 22, no. 2, pp. 111–121, Jan. 2008.

[17] J. Mehrholz, T. Platz, J. Kugler, and M. Pohl, "Electromechanical and robot-assisted arm training for improving arm function and activities of daily living after stroke," *Stroke*, vol. 40, no. 5, pp. 392–393, 2009.

[18] Q. Miao, M. Zhang, J. Cao, and S. Q. Xie, "Reviewing high-level control techniques on robot-assisted upper-limb rehabilitation," *Adv. Robot.*, vol. 32, no. 24, pp. 1253–1268, 2018.

[19] Q. Wu, X. Wang, B. Chen, and H. Wu, "Development of an RBFN-based neural-fuzzy adaptive control strategy for an upper limb rehabilitation exoskeleton," *Mechatronics*, vol. 53, pp. 85–94, Aug. 2018.

[20] J. Niu, Q. Yang, X. Wang, and R. Song, "Sliding mode tracking control of a wire-driven upper-limb rehabilitation robot with nonlinear disturbance observer," *Frontiers Neurol.*, vol. 8, p. 646, Dec. 2017.

[21] S. Mohan, J. K. Mohanta, S. Kurtenbach, J. N. Paris, B. Corves, and M. Huesing, "Design, development and control of a 2 P RP-2 P PR planar parallel manipulator for lower limb rehabilitation therapies," *Mech. Mach. Theory*, vol. 112, pp. 272–294, Jun. 2017.

[22] F. Zhang, L. Lin, L. Yang, and Y. Fu, "Design of an active and passive control system of hand exoskeleton for rehabilitation," *Appl. Sci.*, vol. 9, no. 11, p. 2291, Jun. 2019.

[23] Q. C. Wu, B. Chen, and H. T. Wu, "Adaptive admittance control of an upper extremity rehabilitation robot with neural-network-based disturbance observer," *IEEE Access*, vol. 7, pp. 123807–123819, 2019.

[24] G. G. Peña, L. J. Consoni, W. M. dos Santos, and A. A. G. Siqueira, "Feasibility of an optimal EMG-driven adaptive impedance control applied to an active knee orthosis," *Robot. Autom. Syst.*, vol. 112, pp. 98–108, Feb. 2019.

[25] P. Agarwal and A. D. Deshpande, "Subject-specific assist-as-needed controllers for a hand exoskeleton for rehabilitation," *IEEE Robot. Autom. Lett.*, vol. 3, no. 1, pp. 508–515, Jan. 2018.

[26] A. M. Khan, D.-W. Yun, K. M. Zuhaib, J. Iqbal, R.-J. Yan, F. Khan, and C. Han, "Estimation of desired motion intention and compliance control for upper limb assist exoskeleton," *Int. J. Control Autom.*, vol. 15, no. 2, pp. 802–814, Apr. 2017.

[27] X.-Z. Jiang, X.-H. Huang, C.-H. Xiong, R.-L. Sun, and X.-L. Xiong, "Position control of a rehabilitation robotic joint based on neuron proportion-integral and feedforward control," *J. Comput. Nonlinear Dyn.*, vol. 7, no. 2, Apr. 2012, Art. no. 024502.

[28] Y. Yang, D. Huang, and X. Dong, "Enhanced neural network control of lower limb rehabilitation exoskeleton by add-on repetitive learning," *Neurocomputing*, vol. 323, pp. 256–264, Jan. 2019.

[29] Q. Wu, X. Wang, R. Xi, and F. Du, "Modeling and position control of a therapeutic exoskeleton targeting upper extremity rehabilitation," *Proc. Inst. Mech. Eng. C, J. Mech. Eng. Sci.*, vol. 231, no. 23, pp. 4360–4373, 2017.

[30] A. Riani, T. Madani, A. Benallegue, and K. Djouani, "Adaptive integral terminal sliding mode control for upper-limb rehabilitation exoskeleton," *Control Eng. Pract.*, vol. 75, pp. 108–117, Jun. 2018.

[31] J. Yang, H. Su, Z. Li, D. Ao, and R. Song, "Adaptive control with a fuzzy tuner for cable-based rehabilitation robot," *Int. J. Control Autom.*, vol. 14, no. 3, pp. 865–875, Jun. 2016.

[32] A. U. Pehlivan, D. P. Losey, and M. K. O'Malley, "Minimal assist-as-needed controller for upper limb robotic rehabilitation," *IEEE Trans. Robot.*, vol. 32, no. 1, pp. 113–124, Feb. 2015.

[33] M. Zhang, S. Q. Xie, X. Li, G. Zhu, W. Meng, X. Huang, and A. J. Veale, "Adaptive patient-cooperative control of a compliant ankle rehabilitation robot (CARR) with enhanced training safety," *IEEE Trans. Ind. Electron.*, vol. 65, no. 2, pp. 1398–1407, Feb. 2018.

[34] Z. Li, Y. Kang, Z. Xiao, and W. Song, "Human–robot coordination control of robotic exoskeletons by skill transfers," *IEEE Trans. Ind. Electron.*, vol. 64, no. 6, pp. 5171–5181, Jun. 2016.

[35] Q. Wu, X. Wang, B. Chen, and H. Wu, "Development of a minimal-intervention-based admittance control strategy for upper extremity rehabilitation exoskeleton," *IEEE Trans. Syst., Man, Cybern., Syst.*, vol. 48, no. 6, pp. 1005–1016, Jun. 2018.

[36] V. Khoshdel and T. A. Akbarzadeh, "Robust impedance control for rehabilitation robot," *Modares Mech. Eng.*, vol. 15, no. 8, pp. 429–437, Oct. 2015.

[37] A. Song, L. Pan, G. Xu, and H. Li, "Adaptive motion control of arm rehabilitation robot based on impedance identification," *Robotica*, vol. 33, no. 9, pp. 1795–1812, Nov. 2015.

[38] G. Xu, A. Song, and H. Li, "Adaptive impedance control for upper-limb rehabilitation robot using evolutionary dynamic recurrent fuzzy neural network," *J. Intell. Robot. Syst.*, vol. 62, no. 3, pp. 501–525, 2011.

[39] H. P. H. Anh, N. N. Son, and C. Van Kien, "Adaptive neural compliant force-position control of serial PAM robot," *J. Intell. Robot. Syst.*, vol. 89, no. 3, pp. 351–369, 2018.

[40] S.-J. Cho, M. Jin, T.-Y. Kuc, and J. S. Lee, "Control and synchronization of chaos systems using time-delay estimation and supervising switching control," *Nonlinear Dyn.*, vol. 75, no. 3, pp. 549–560, Feb. 2014.

[41] J. Kim, H. Joe, S. C. Yu, J. S. Lee, and M. Kim, "Time-delay controller design for position control of autonomous underwater vehicle under disturbances," *IEEE Trans. Ind. Electron.*, vol. 63, no. 2, pp. 1052–1061, Feb. 2016.

[42] J. Baek, S. Cho, and S. Han, "Practical time-delay control with adaptive gains for trajectory tracking of robot manipulators," *IEEE Trans. Ind. Electron.*, vol. 65, no. 7, pp. 5682–5692, Jul. 2018.

[43] J. Lee, C. Yoo, Y.-S. Park, B. Lee, S.-J. Lee, D.-G. Gweon, and P.-H. Chang, "An experimental study on time delay control of actuation system of tilt rotor unmanned aerial vehicle," *Mechatronics*, vol. 22, no. 2, pp. 184–194, Mar. 2012.

[44] B. Brahmi, M. Saad, C. Ochoa-Luna, M. H. Rahman, and A. Brahmi, "Adaptive tracking control of an exoskeleton robot with uncertain dynamics based on estimated time-delay control," *IEEE/ASME Trans. Mechatronics*, vol. 23, no. 2, pp. 575–585, Apr. 2018.

[45] S. Han, H. Wang, and Y. Tian, "Model-free based adaptive nonsingular fast terminal sliding mode control with time-delay estimation for a 12 DOF multi-functional lower limb exoskeleton," *Adv. Eng. Softw.*, vol. 119, pp. 38–47, May 2018.

[46] Z. Chen, Y.-J. Pan, and J. Gu, "Integrated adaptive robust control for multilateral teleoperation systems under arbitrary time delays," *Int. J. Robust Nonlinear Control*, vol. 26, no. 12, pp. 2708–2728, Aug. 2016.

[47] S. Kim and J. Bae, "Force-mode control of rotary series elastic actuators in a lower extremity exoskeleton using model-inverse time delay control," *IEEE/ASME Trans. Mechatronics*, vol. 22, no. 3, pp. 1392–1400, Jun. 2017.
[48] Q. Wu, X. Wang, B. Chen, and H. Wu, "Modeling, online identification, and compensation control of single tendon sheath system with time-varying configuration," *Mech. Syst. Signal Process.*, vol. 130, pp. 56–73, Sep. 2019.
[49] Z. Lu, S. Kawamura, and A. A. Goldenburg, "An approach to sliding-mode based control," *IEEE Trans. Robot. Autom.*, vol. 11, no. 5, pp. 754–759, Oct. 1995.
[50] S. Jung, T. C. Hsia, and R. G. Bonitz, "Force tracking impedance control of robot manipulators under unknown environment," *IEEE Trans. Control Syst. Technol.*, vol. 12, no. 3, pp. 474–483, May 2004.
[51] M. Jin, J. Lee, P. H. Chang, and C. Choi, "Practical nonsingular terminal sliding-mode control of robot manipulators for high-accuracy tracking control," *IEEE Trans. Ind. Electron.*, vol. 56, no. 9, pp. 3593–3601, Sep. 2009.
[52] G. Matthews and R. Decarlos, "Decentralized tracking for a class of interconnected nonlinear systems using variable structure control," *Automatica*, vol. 24, no. 2, pp. 187–193, 1988.
[53] M. Van, H.-J. Kang, and K.-S. Shin, "Backstepping quasi-continuous high-order sliding mode control for a Takagi–Sugeno fuzzy system with an application for a two-link robot control," *Proc. Inst. Mech. Eng., C, J. Mech. Eng. Sci.*, vol. 228, no. 9, pp. 1488–1500, 2014.
[54] T. D. Le, H.-J. Kang, and Y.-S. Suh, "Chattering-free neuro-sliding mode control of 2-DOF planar parallel manipulators," *Int. J. Adv. Robot. Syst.*, vol. 10, no. 1, p. 22, Jan. 2013.
[55] Q. Wuet, X. Wang, B. Chen, H. Wu, and Z. Shao, "Development and hybrid force/position control of a compliant rescue manipulator," *Mechatronics*, vol. 46, pp. 143–153, Oct. 2017.
[56] J. E. Slightam, M. L. Nagurka, and E. J. Barth, "Sliding mode impedance control of a hydraulic artificial muscle," in *Proc. ASME Int. Conf. Dyn. Syst. Control.*, Sep. 2018, p. V001T13A003.

**QINGCONG WU** received the B.S. and Ph.D. degrees in mechatronics engineering from Southeast University, Nanjing, China, in 2011 and 2016, respectively. He is currently an Assistant Professor with the College of Mechanical and Electrical Engineering, Nanjing University of Aeronautics and Astronautics, Nanjing. His research interests include robotics, human–robot interaction control, tendon-sheath transmission theory, gravity balancing theory, and the application of exoskeleton to neuromuscular rehabilitation.

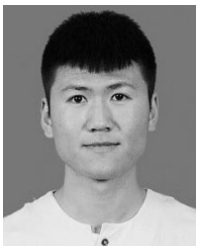

**DAWEN XU** received the B.S. degree in mechatronics engineering from Suzhou University, Suzhou, China, in 2018. He is currently pursuing the M.S. degree in mechatronics engineering with the College of Mechanical and Electrical Engineering, Nanjing University of Aeronautics and Astronautics, Nanjing, China. His research interests include rehabilitation robot, human–robot interaction control, and soft exoskeleton.

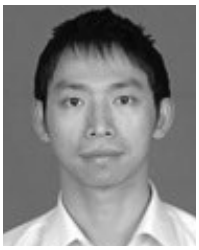

**BAI CHEN** received the B.S. and Ph.D. degrees in mechanical engineering from Zhejiang University, Hangzhou, China, in 2000 and 2005, respectively. He is currently a Full Professor with the College of Mechanical and Electrical Engineering, Nanjing University of Aeronautics and Astronautics. His current research interests include minimally invasive neurosurgery robot, virtual surgery system, force feedback control, and interventional therapy.

**HONGTAO WU** received the B.S. degree from Yanshan University, Hebei, China, in 1982, and the M.S. and Ph.D. degrees from Tianjin University, Tianjin, China, in 1985 and 1992, respectively, all in mechanical engineering. He is currently a Full Professor with the College of Mechanical and Electrical Engineering, Nanjing University of Aeronautics and Astronautics. His current research interests include parallel robot, robot kinematics, and multibody system dynamics.